Selective and uncoupled role of substrate elasticity in the regulation of replication and transcription in epithelial cells

Leyla Kocgozlu[1,2,3], Philippe Lavalle[1,2,4], Géraldine Koenig[1,2], Bernard Senger[1,2], Youssef Haikel[1,2,3], Pierre Schaaf[5], Jean-Claude Voegel[1,2,3], Henri Tenenbaum[1,2,3] and Dominique Vautier[1,2,3,*]

[1]Institut National de la Santé et de la Recherche Médicale, INSERM Unité 977, 67085 Strasbourg Cedex, France
[2]Faculté de Chirurgie Dentaire, Université de Strasbourg, 67000 Strasbourg, France
[3]Equipe de Recherche Technologique 10-61 interne à l'unité 977, 67085 Strasbourg Cedex, France
[4]Hôpitaux Universitaires de Strasbourg, 67000 Strasbourg, France
[5]Centre National de la Recherche Scientifique, UPR22, Institut Charles Sadron, BP 84047, 67034 Strasbourg Cedex, France
*Author for correspondence (Dominique.Vautier@medecine.u-strasbg.fr)

Accepted 2 October 2009
Journal of Cell Science 123, 29-39 Published by The Company of Biologists 2010
doi:10.1242/jcs.053520

Summary

Actin cytoskeleton forms a physical connection between the extracellular matrix, adhesion complexes and nuclear architecture. Because tissue stiffness plays key roles in adhesion and cytoskeletal organization, an important open question concerns the influence of substrate elasticity on replication and transcription. To answer this major question, polyelectrolyte multilayer films were used as substrate models with apparent elastic moduli ranging from 0 to 500 kPa. The sequential relationship between Rac1, vinculin adhesion assembly, and replication becomes efficient at above 200 kPa because activation of Rac1 leads to vinculin assembly, actin fiber formation and, subsequently, to initiation of replication. An optimal window of elasticity (200 kPa) is required for activation of focal adhesion kinase through auto-phosphorylation of tyrosine 397. Transcription, including nuclear recruitment of heterogeneous nuclear ribonucleoprotein A1 (hnRNP A1), occurred above 50 kPa. Actin fiber and focal adhesion signaling are not required for transcription. Above 50 kPa, transcription was correlated with αv-integrin engagement together with histone H3 hyperacetylation and chromatin decondensation, allowing little cell spreading. By contrast, soft substrate (below 50 kPa) promoted morphological changes characteristic of apoptosis, including cell rounding, nucleus condensation, loss of focal adhesions and exposure of phosphatidylserine at the outer cell surface. On the basis of our data, we propose a selective and uncoupled contribution from the substrate elasticity to the regulation of replication and transcription activities for an epithelial cell model.

Key words: Substrate elasticity, Integrin, Actin, Vinculin, Rac1, Replication, Transcription

Introduction

Cell activity in vivo is largely dependent on the properties of the surrounding tissue, where numerous biochemical and mechanical cues originate. For instance, during their development, neuronal crate cells cross different extracellular stroma. To colonize targeting organs, circulating lymphocytes cross several tissues. Also, in pathological processes such as metastastic disseminations, tumor cells acquire the ability to migrate into the stroma. Up to now, extracellular matrix (ECM)-cell interactions driving these various processes have generally been investigated using biochemical approaches. These in vitro studies are often performed on plastic or glass dishes, which constitute stiffer surfaces than the stiffest living tissues. Moreover, various substrates (e.g. isoform laminin, collagen I/IV etc.) interact with different types of receptors to activate various signaling pathways, ultimately resulting in different cell responses (Gross et al., 2008). However, little is known about the consequences on cell behavior of varying physical parameters of the cell microenvironment. Major cellular events take place within the nucleus, including replication, messenger RNA synthesis and processing, and ribosome subunit biogenesis. How mechanical matrix information transmitted through the cytoskeleton can affect both structure and function within the nucleus is a matter of great debate (Gieni and Hendzel, 2008). 'Tensegrity' models postulated how mechanical forces, generated through cell-ECM interactions via focal adhesions (FAs) could impact cytoskeletal and nuclear morphology and ultimately induce changes in the pattern of gene expression (Wang et al., 2009). Conversion of mechanical information into a cellular signal is mediated by the actin cytoskeleton through interactions between integrins and actin-binding proteins (talin, paxillin, vinculin). Matrix compliance influences cytoskeletal tensions, Rho activity and ERK-dependent growth (Wang et al., 1998; Wozniak et al., 2003), with cytoskeletal tension promoting growth (Roovers and Assoian, 2003) and FA assembly (Burridge and Wennerberg, 2004). Investigation of the mechanoregulatory circuit, via ERK and Rho activities, linking matrix stiffness to cytoskeletal tension through integrins (to regulate tissue phenotype), has become an emerging research domain (Paszek et al., 2005). Close to the nuclear sites of transcription, different hypothetical models can account for transmission of mechanical signals directly to the nuclear sites of transcription: First, chromatin is connected to the nuclear lamina through a putative karyoskeleton; and second, chromatin interacts directly with the nuclear lamina and slicing factor compartment (Maxwell and Hendzel, 2001). This second hypothesis has been verified (Shimi et al., 2008). Nucleoplasmic lamin A, localized at the nuclear envelope blebs, is associated with gene-rich euchromatin, together with RNA polymerase II and histone, creating conditions for active transcription (Shimi et al., 2008). Yet, the fundamental question

Journal of Cell Science

that remains unanswered is whether replication and transcription at the nucleospatial organizational level are influenced by the substrate elasticity. This constitutes the central issue of this paper.

The Young modulus, E (deformation properties under stress are usually reported in pascals), of living tissues exhibits a wide range of values (Levental et al., 2007). Brain, for example, has a Young modulus of several hundred pascals, whereas that of muscle lies above 10 kPa. Tissue from kidney has a value around 100 kPa and that of tendon and cartilage is in the range of megapascals (Levental et al., 2007; Georges et al., 2006; Snedeker et al., 2005; Engler et al., 2004; Discher et al., 2005). Only recently have proposals been made for more compliant materials that have tunable elasticity values that are comparable to living tissue. For instance, gels of polyacrylamide (PA) (Pelham and Wang, 1997; Lo et al., 2000; Engler et al., 2004; Yeung et al., 2005), matrices of polydimethylsiloxane (Wong et al., 2003), polyethylene glycol (Rizzi et al., 2006) and polyelectrolyte multilayers (PEMs) (Decher, 1997) all offer the opportunity to study cellular behavior under well-defined mechanical conditions (Richert et al., 2004; Ren et al., 2008). Pelham and Wang, using PA gels of variable stiffness as substrates, observed that epithelial cells and fibroblasts exhibit differences in motility and FA organization (Pelham and Wang, 1997). Mesenchymal stem cells could express key markers of neurogenic, myogenic and osteogenic lineages once they were cultured on PA gels with stiffness values that corresponded to the tissue elasticities of brain (1 kPa), muscle (10 kPa) and nascent bone (100 kPa) (Engler et al., 2006).

The goal of the present work was to investigate the influence of the rheological substrate properties on adhesion signaling pathways as well as on DNA replication and transcription. We also examined whether correlations exist between adhesion pathways, replication and transcription. We used PEMs, namely hyaluronic acid/poly-L-lysine (HA/PLL) capped with poly(styrene) sulfonate/polyallylamine hydrochloride (PSS/PAH) multilayers as the substrate models (Garza et al., 2004). The alternate deposition of positively and negatively charged polyelectrolytes onto solid substrates leads to the formation of nanostructured films known as PEMs (Decher, 1997). HA/PLL is known to be non-adhesive to cells (Mendelsohn et al., 2003), whereas PSS/PAH presents remarkable properties with respect to cell adhesion and cellular proliferation (Boura et al., 2005). The origin of these remarkable properties is still unknown but is expected to be related to the mechanical properties of PSS/PAH. The HA/PLL films capped with PSS/PAH allow modulation of these mechanical properties. These films, in contrast to reticulated gels, are not only elastic but also viscoelastic. The viscoelasticity of these films was explored by Francius and colleagues (Francius et al., 2007) using atomic force microscopy (AFM). This technique, however, only allows exploration of a time scale from 10 to 10^{-3} seconds. Longer times might be involved in cellular adhesion or other physiological cellular processes (Engler et al., 2008) but cannot be explored experimentally by this technique. What is firmly established is that the higher the number of PSS/PAH layers, the stiffer the film becomes. We characterized the films by their apparent elastic modulus (E_{ap}), which would correspond to the real elastic modulus of the layer if it behaved strictly elastically. The E_{ap} value should, therefore, not be taken in a strict sense when comparing it to other published systems, but as a semi-quantitative estimation of the stiffness. The response of the cells depends on the changes in the stiffness of the polyelectrolyte multilayers, showing the biological relevance of this mechanical parameter that characterizes the films. On the basis of previous work, marsupial kidney epithelial (PtK2) cells were chosen as a model for following the spatial configuration of replication and transcriptional (Ferreira et al., 1997).

Results

Progressive stiffening of the PEM films increases cell adhesion

PEM films were used to investigate how the mechanical properties of the substrate might play a role in replication and transcription activities at the nucleo-spatial organizational level. The films were composed of a $(PLL/HA)_{24}$ stratum capped by a second $(PSS/PAH)_n$ stratum (n=0, 2, 5 and 12). A typical example of confocal z-section observation of a film composed of PLL/HA stratum and PSS/PAH capping is displayed in Fig. 1Aa. Note that for n=0, the film corresponds to a PLL/HA film that is essentially a viscous liquid (Picart et al., 2007) and unfavorable for cell adhesion (Mendelsohn et al., 2003). By contrast, the values of the elastic moduli for the set of $(PSS/PAH)_n$ strata lie in the gigapascal range (Dubreuil et al., 2003). However, as the number of capping layers increases, the film becomes stiffer, as we previously showed by AFM indentation experiments (Francius et al., 2007). Although the PLL/HA stratum is capped, the whole film behaves like a viscoelastic medium. Each of the films was modeled as a spring (elastic modulus E_1) in series with a Kelvin unit, which is itself a spring (elastic modulus E_2), in parallel with a dashpot. We will refer to this model as the SK model (where S stands for spring and K for Kelvin). Fig. 1Ab shows the effect of depositing PSS and PAH on top of the PLL/HA stratum, and represents the evolution of the apparent elastic modulus in the SK model ($1/E_{ap}=1/E_1 + 1/E_2$) at a given expansion velocity (about 1 μm/second) for the AFM piezodrive. It follows from Fig. 1Ab that the apparent moduli are roughly 50, 200 and 500 kPa for the architectures $(PLL/HA)_{24}$-$(PSS/PAH)_n$ with n=2, 5, 12, respectively. It is known from earlier investigations (Francius et al., 2006) that the elastic modulus of the native $(PLL/HA)_{24}$ architecture is under 1 kPa and is considered here as our zero. Henceforth, we shall use the short-hand notations E0, E50, E200 and E500 for the $(PLL/HA)_{24}$, $(PLL/HA)_{24}$-$(PSS/PAH)_n$ films with n=2, 5, 12, respectively, and 0/2, 0/5 and 0/12 for $(PSS/PAH)_2$, $(PSS/PAH)_5$ and $(PSS/PAH)_{12}$ films, respectively (see Table 1). Also, the amount of ligands adsorbed from the serum was quantified using a quartz crystal microbalance. Supplementary material Table S1 summarizes these results. The amount of ligands deposited from 10% fetal bovine serum (FBS) does not depend on the number of polyelectrolyte layers deposited on the surface.

The adhesion of PtK2 cells was first investigated 4 hours (a sufficient time for onset of nuclear activities) after seeding on the different film architectures using the MTT test (see Materials and Methods). As seen in Fig. 1B, adhesion of cells cultured on 0/2, 0/5 and 0/12 films was almost the same as that observed for bare glass surface. This observation is expected because the values of elastic moduli for all these surfaces lie within the gigapascal range (Dubreuil et al., 2003). Progressive decrease in cell adhesion was observed when cells were seeded onto substrates for which stiffness progressively decreased (Fig. 1B; E50 and E0 films compared to glass). A similar cell-film adhesion response was obtained using the acid phosphatase test (supplementary material Fig. S1).

Organization of actin fibers and vinculin assembly require substrate elasticity of above 200 kPa

To determine whether αv-integrins, organization of actin fibers and vinculin FA assembly were affected by the film stiffness,

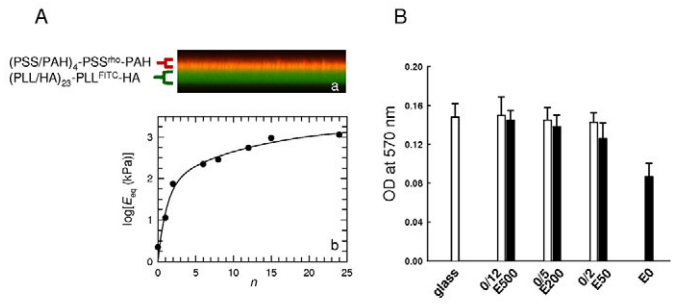

Fig. 1. PEM films and cell adhesion. (**Aa**) Vertical section image of a $(PLL/HA)_{23}$-PLL^{FITC}-HA–$(PSS/PAH)_4$-PSS^{Rho}-PAH multilayered film observed by CLSM. (**Ab**) Decimal logarithm of E_{ap} of $(PLL/HA)_{24}$-$(PSS/PAH)_n$ and -PSS films investigated previously (Francius et al., 2007) as a function of the number (n) of (PSS or PAH) layers. (**B**) Results of Mtt test after 4 hours of adhesion on glass surface (glass) or on E0, E50, E200, E500, 0/2, 0/5 and 0/12 films. Error bars represent s.d. derived from two independent experiments (triplicate well determinations, four measurements per well).

Table 1. Ea of $(PLL/HA)_{24}$-$(PSS/PAH)_n$ with n=2, 5, 12

Architecture	Eap* (kPa)	Notation
$(PLL/HA)_{24}$	~0	E0
$(PLL/HA)_{24}$-$(PSS/PAH)_2$	~50	E50
$(PLL/HA)_{24}$-$(PSS/PAH)_5$	~200	E200
$(PLL/HA)_{24}$-$(PSS/PAH)_{12}$	~500	E500
$(PSS/PAH)_2$	NA	0/2
$(PSS/PAH)_5$	NA	0/5
$(PSS/PAH)_{12}$	NA	0/12

Eap was determined by AFM nano-indentation. NA, non-available.
*Values from Francius et al. (Francius et al., 2007).

immunofluorescence experiments using antibodies specific for integrin, and phalloidin staining for F-actin and vinculin, were performed on cells cultured for 4 hours on the stiffened substrates. Cells cultured on E500 and E200 films all displayed peripheral αv-integrin spots (Fig. 2Aa,d) and localized at the tip of actin microfilaments (Fig. 2Ab,e) and vinculin sites (Fig. 2Ac,f), similarly to the well-known pattern described in cells grown on glass and on 0/2, 0/5 and 0/12 films (supplementary material Fig. S2Aa,c,e,g for F-actin and supplementary material Fig. S2Ab,d,f,h for vinculin). By contrast, neither αv-integrin spots, F-actin stress fibers nor vinculin adhesion spots were detected in cells cultured on E0 (Fig. 2Aj-l) or E50 films (Fig. 2Ah,B for F-actin and Fig. 2Ai for vinculin). However, on E50 films, αv-integrin spots were visualized (Fig. 2Ag). These results clearly indicate that actin-fiber organization and vinculin FA assembly require a substrate whose E_{ap} exceeds 50 kPa.

Activation of FAK-Y397 takes place at an optimal elastic modulus

The adhesion process is a complex cascade of reactions, and focal adhesion kinase (FAK) is one of the major kinases implicated in FA-contact signaling. FAK is activated and localized at FA contacts after cell adhesion to the extracellular matrix (Schaller et al., 1999). Integrin engagement initiates auto-phosphorylation of tyrosine 397 (FAK-Y397) (Kornberg et al., 1991). Accordingly, we have investigated whether film stiffness also affects FAK-Y397 auto-phosphorylation. Using specifically directed antibodies, we used western blot to analyze phosphorylated FAK-Y397 (FAK-Y397-*P*) expressed by cells cultured for 4 hours on substrates of increasing stiffness. Western blots are given in Fig. 2C. Cells cultured on E0

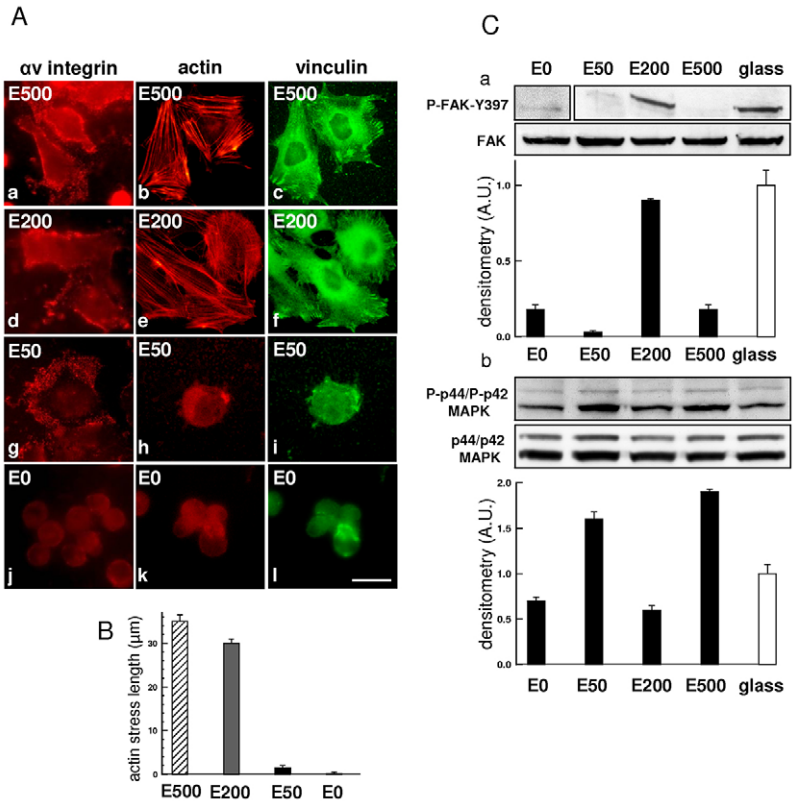

Fig. 2. αv-integrin, actin fiber, vinculin and activation of FAK-Y397 at different substrate elasticities. (**A**) Images of cells after 4 hours of culture on E500 (a-c), E200 (d-f), E50 (g-i) and E0 (j-l) with anti-αv-integrin (a,d,g,j), labeled with phalloidin (b,e,h,k) or anti-vinculin (c,f,i,l). Scale bar: 20 µm. (**B**) Quantification of actin stress (in µm) using ImageJ, based on Ab,e,h,k and obtained by measuring the length of 20 actin stress fibers per cell for 20 cells. Results are presented as s.e.m. for three independent experiments. (**Ca**) Western blots of FAK and phosphorylated FAK-Y397 (P-FAK-Y397) in cells seeded 4 hours on E0, E50, E200, E500 films and glass. Histogram shows the corresponding scans for phosphorylated FAK-Y397. (**Cb**) Western blots of p44/p42 MAPK and phosphorylated p44/p42 MAPK (P-p44/p42 MAPK) in cells seeded 4 hours on E0, E50, E200, E500 films and glass. Histogram shows the corresponding scans for phosphorylated p44/p42 MAPK. Representative results from at least three independent experiments.

and on E50 films failed to induce activation of FAK-Y397, whereas the protein was activated on E200 films (Fig. 2Ca and supplementary material Fig. S2Ba). Surprisingly, cells cultured on E500 films (an even stiffer substrate) also failed to induce activation of FAK-Y397 (Fig. 2Ca and supplementary material Fig. S2Bb), whereas, on harder strata 0/2, 0/5 and 0/12 (supplementary material Fig. S2C) and on a glass surface (Fig. 2Ca) FAK-Y397-*P* was activated. These observations suggest that activation of FAK-Y397-*P* takes place in a finite range at an optimal elastic modulus (around 200 kPa) and also for stiff material. Following FAK activation, a kinase signaling cascade leads to stimulation of p42/p44 MAPK (also called ERK1 and ERK2), which is required for cell migration, survival and gene expression (Huang et al., 2004). Thus, the activation of p42/p44 MAPK in response to substrate elasticity was investigated. Fig. 2Cb shows that cell incubation on E0, E50, E200 and E500 films allowed activation of phosphorylated p44/p42 MAPK. This result suggests that substrate elasticity ranging from 1 to 500 kPa is not an environmental parameter able to inhibit activation of phosphorylated p44/p42 MAPK.

Inhibition of replication is strongly correlated with inhibition of vinculin assembly

Focal adhesion morphology is thought to be dependent on the cell-cycle phase. FA sites are small and numerous in non-S-phase periods, yet mature and less numerous in S phase (Meredith et al., 2004). In S phase, nucleosides are incorporated into the DNA of the cell and a duplicate set of chromosomes is synthesized (Pardee, 1989).

A major question is then whether or not DNA replication can be affected by the stiffness of the substrate in correlation with assembly of vinculin FAs. To address this question, we synchronized a collection of cells using the mitotic shake-off method to chronologically follow the initial steps of vinculin FA-site organization in relation to the onset of DNA replication. These time-dependent events were first analyzed on a control surface (glass substrate). Then, we investigated on E50 films whether altering one event had any consequences on another with respect to cell progression through the ongoing cell cycle. The influence of substrate elasticity on these time-dependent events was also checked for E200 and E500 films. On glass substrate, cells re-attached as early as 30 minutes after release. Within 1-2 hours after synchronization, cells had progressively spread over the surface (Fig. 3A,Ba shows round-shaped morphologies at 1 hour; Fig. 3Bb, show spread morphologies at 2 hours). At 2 hours after synchronization, neither punctuate vinculin staining (Fig. 3Bb) nor replication activities were detected in cells (Fig. 3Bi). Vinculin FA assembly was first visible 3 hours after mitosis. These vinculin spots were uniformly distributed at the periphery of cells (Fig. 3Bc), reaching a length of 1.6±0.03 μm (Fig. 3E). These spots were assigned to focal complexes and originated as dot-like structures (Biggs et al., 2007). During this time period, DNA replication was still inactive (Fig. 3Bj). BrdU incorporation sites were first detected 4 hours after synchronization (Fig. 3Bk,F) while the vinculin spots increased in length (3 μm) (Fig. 3Be,E). Within 5-7 hours post-mitosis, cells reached a maximum area of about 1300 μm^2 (Fig. 3A) and displayed vinculin spots of increased length (4 μm) (Fig. 3E), preferentially localized at the cell protrusive extremities (Fig. 3Be-g). These spots were assigned to mature FAs. Mature FAs are typically dash-shaped with areas of 2-5 μm^2. Mature FAs were identified as structures containing vinculin, paxillin, and talin (Biggs et al., 2007). At this time, cells still remained in S phase (Fig. 3Bl-n and Fig.3F; total S phase duration was about 10 hours) (Mitchison, 1971). Release of cells onto E50 films did not affect reattachment but did reduce cell spreading (Fig. 3A,C) and inhibit the formation of vinculin structures (Fig. 3Ca-g). In addition, DNA replication was completely obstructed throughout the time period normally required to observe this activity (Fig. 3Ck-n,F). Taken together, these results seem to indicate that inhibition of replication is strongly correlated with the inhibition of vinculin assembly. For E200 and E500 films, at 1-7 hours post-synchronization, the cell area remained smaller than area values on glass surface (Fig. 3A; 5-7 hours post-synchronization 1000 μm^2 for E200, 950 μm^2 for E500 and 1300 μm^2 for glass). Vinculin structures were detected 3 hours after mitosis on the E200 and E500 films (Fig. 3Dc,E and supplementary material Fig. S3Bc). On E200 and on E500 films, after 5-7 hours post-synchronization, vinculin spots were smaller at the cell protrusive extremity (Fig. 3De-g,E, 2.8 μm for E200 films; Fig. 3E, 2.6 μm for E500 films; supplementary material Fig. S3Be-g) than those visualized on glass surface (Fig. 3Be-g,E, approximately 4 μm). However, even for these two architectures, vinculin spots (length greater than 2 μm) could still be assigned to 'dash' structures. For E200 and E500 films, replication took place 4 hours after mitotic synchronization (Fig. 3Dk-n for E200 films; supplementary material Fig. S3Bk-n for E500 films; and Fig. 3F for quantification). These results demonstrate that vinculin assembly depends on the elastic modulus of the surface (200 kPa) and precedes cell progression into S phase. Interestingly, on control surface (glass surface), the kinetics of vinculin FA assembly (3 hours post-mitosis) and onset of replication (4 hours post-mitosis) were identical to those observed when a substrate reached an elastic modulus value above the 200 kPa necessary and sufficient for vinculin assembly and replication.

Rac1 activity requires substrate elasticity above 200 kPa to regulate vinculin assembly, actin stress and replication

Rac1 is member of the ras-related superfamily of small GTPases that regulate both polymerization of actin to produce lamellipodia and vinculin FA assembly at the plasma membrane (Nobes and Hall, 1995). To try to establish direct relationships and whether inhibition of replication can be attributed to inhibition of vinculin assembly, we tested the influence of substrate elasticity on Rac1 activity with or without the anti-Rac1 inhibitor NSC23766. In cells synchronized by mitotic shake-off, Rac1 was cytoplasmic after 3 hours on glass (supplementary material Fig. S4a), E500 (supplementary material Fig. S4d) and E200 (Fig. 4Aa) substrates; 4 hours on glass (supplementary material Fig. S4b), E500 (supplementary material Fig. S4e) and E200 substrates (Fig. 4Ab); and 7 hours after synchronization on glass (supplementary material Fig. S4c), E500 (supplementary material Fig. S4f) and E200 substrates (Fig. 4Ac). By contrast, Rac1 was not detected on E0 (data not shown) nor E50 film at 3, 4 and 7 hours after synchronization (Fig. 4Ad-f and Fig. 4B). In the presence of the inhibitor NSC23766, Rac1 was not detected at 3, 4 and 7 hours after synchronization (Fig. 4Ag-i and Fig. 4B). Interestingly, at 3, 4 and 7 hours after synchronization, the inhibition of Rac1 by the drug concomitantly obstructed vinculin (Fig. 4Aj-l and Fig. 4C), actin (Fig. 4Am-o and Fig. 4C) and replication on E200 film (Fig. 4Ap-r and Fig. 4D) or glass substrate (data not shown). These results strongly suggest that Rac1 could be a signaling pathway sequentially linking vinculin, formation of actin stress fibers and replication.

Uncoupled contribution from the substrate elasticity to the regulation of replication and transcription

In recent studies it was postulated that mechanical signals from the extracellular environment could be transduced to the nucleus via

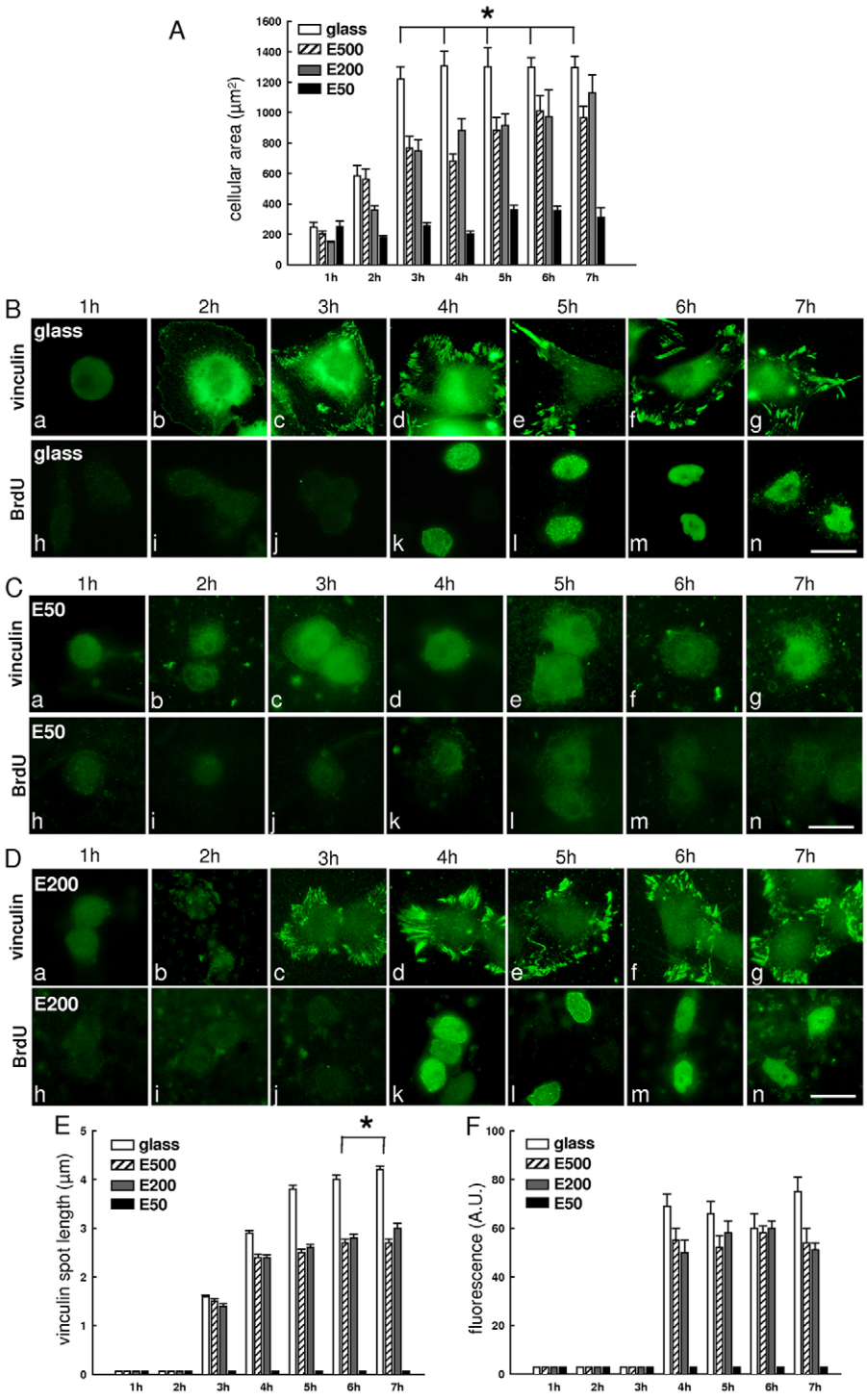

Fig. 3. Vinculin assembly and replication for different substrates with respect to mitotic synchronization. (**A**) Quantitative data of cell areas (in μm^2), based on Ba-g, Ca-g, Da-g and supplementary material Fig. S3Ba-g, were determined using ImageJ. 200-300 cells were used for each condition (E50, E200, E500 films and glass surface) for seven time periods. Results are presented as s.e.m. for three independent experiments; *statistically no significant difference (P<0.01, ANOVA on rank). (**B-D**) Cells seeded on glass surface (B), E50 (C) and E200 (D) were fixed 1-7 hours after synchronization. Images show cells with anti-vinculin (a-g) and BrdU visualized by indirect immunofluorescence (h-n). Scale bar: 20 μm. (**E**) Quantification of vinculin spots (in μm), based on Ba-g, Ca-g, Da-g and supplementary material Fig. S3Ba-g, were obtained by measuring 20 contacts per cell for 20 post-mitotic cells (for seven time periods). Results are presented as s.e.m. for three independent experiments; *statistically not significant difference (P<0.05, Dunn's method). (**F**) Fluorescence intensity for nuclear BrdU signal (arbitrary units, A.U. in %) using ImageJ, based on Bh-n, 3Ch-n, 3Dh-n and supplementary material Fig. S3Bh-n. Results were determined on 50 cells (for seven time periods) and are presented as s.e.m. for three independent experiments.

morphological changes. These changes can open or close areas of DNA near to the transcription site (Dalby et al., 2007; Gieni and Hendzel, 2008). With this in mind, it seemed appropriate to determine whether the stiffness of the substrate influences the transcriptional activity in the nucleus. Transcription sites were detected by labeling nascent transcripts with bromouridine (BrU). For somatic cells in culture, because transcription starts within minutes of completing mitosis and assembling daughter nuclei (Ferreira et al., 1994), the nascent RNA labeling method was applied to unsynchronized cells. Cells cultured for 4 hours on an E0 film showed a total absence of transcription sites (Fig. 5Aa,B). On these substrates, the nuclei in these PtK2 cells were transcriptionally silent. By contrast, cells cultured on E50 films displayed sites of transcription uniformly distributed in the nucleus (Fig. 5Ac,B). The same observation holds for E200 and E500 substrates (Fig. 5Ae,g and Fig. 5B) and also for 0/2, 0/5 and 0/12 films and a glass surface (supplementary material Fig. S5Aa-d). To confirm the influence of substrate elasticity on the transcriptional competence observed in unsynchronized cells cultured on the E50, we also investigated actin-fiber organization and transcription for 4 hours post-synchronization

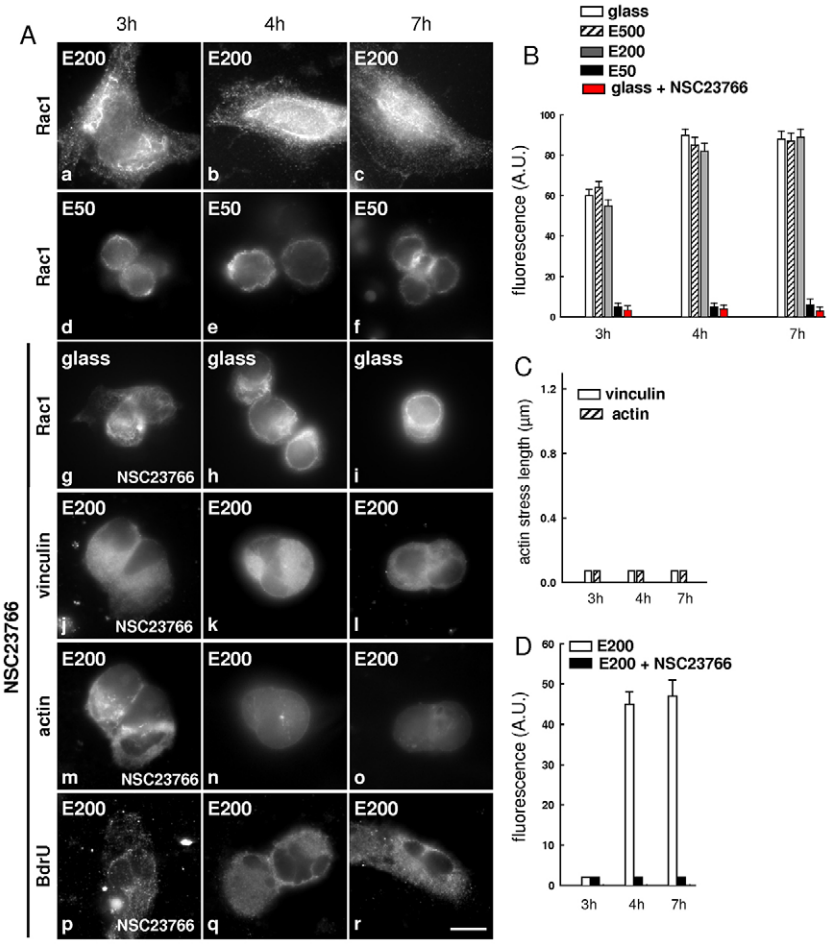

Fig. 4. Rac 1 activity with respect to elastic modulus. (**A**) Cells were seeded on E200, E50 and glass. Images show cells with anti-Rac1 (a-i), anti-vinculin (j-l), labeled with phalloidin (m-o), and BrdU visualized by indirect immunofluorescence (p-r). Cells were fixed 3, 4 and 7 hours after synchronization. For Rac1 inhibitor treatment, cells were cultured with 100 µM NSC 23766 (g-r) until their fixation. Scale bar: 20 µm. (**B**) Fluorescence intensity for Rac1 signal (arbitrary units, A.U. in %) using ImageJ, based on Aa-i. 200 cells per condition were analyzed. Results are presented as s.e.m. for two independent experiments. (**C**) Quantification of vinculin spots and actin stress (in µm), based on Aj-l and Am-o, respectively, obtained by measuring the length of 20 contacts per cell for 20 post-mitotic cells (for three time periods). Results are presented as s.e.m. for two independent experiments. (**D**) Fluorescence intensity for nuclear BrdU signal (arbitrary units, A.U. in %) using ImageJ, based on Ap-r; determined on 50 cells (for three time periods).

on the E50 substrate. Under these conditions, although formation of actin fibers was inhibited (Fig. 5Ca,D), cells displayed transcription sites uniformly distributed in the nucleus (Fig. 5Cb,D). Very importantly, this result shows that transcriptional activity does not require the actin fiber cytoskeleton because it is absent on the E50 substrates. Furthermore, it does not require vinculin assembly and activation of FAK-Y397.

Nuclear transcriptional competence was also assessed following the nucleocytoplasmic distribution of the heterogeneous nuclear ribonucleoprotein A1 (hnRNP A1). Indeed, hnRNP A1 involved in RNA processing (reviewed in Dreyfuss et al., 1993) is an indirect transcriptional marker because its nuclear accumulation is inhibited by the presence of RNA polymerase II transcription inhibitors, implying a link between transport and transcriptional activity (Piñol-Roma and Dreyfuss, 1991; Vautier et al., 2001). Cells cultured on E0 films showed that hnRNP A1 protein accumulated in cytoplasm

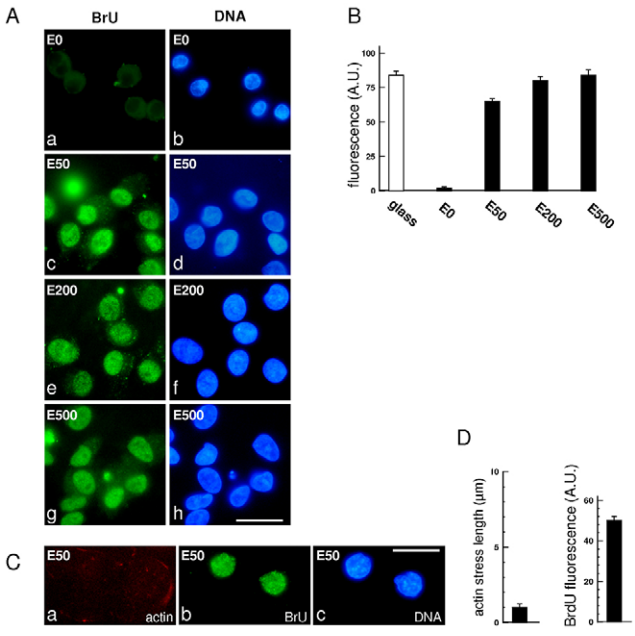

Fig. 5. Transcription with respect to substrate elasticity. (**A**) Cells cultured for 4 hours on E0, E50, E200 and E500 films with anti-BrU (a,c,e,g) and counterstained with Hoechst 33258 (b,c,f,h). Scale bar: 20 µm. (**B**) Fluorescence intensity for nuclear BrU signal (arbitrary units, A.U. in %) using ImageJ, based on Aa,c,e,g; 300 cells per condition were analyzed. Results are presented as s.e.m. for three independent experiments. (**C**) On E50 films, cells were fixed 4 hours after synchronization and labeled with phalloidin (a), immunolabeled with anti-BrU (b), and counterstained with Hoechst 33258 (c). Scale bar: 20 µm. (**D**) Quantification of actin stress (in µm) using ImageJ, based on image Ca, by measuring the length of 20 actin stress fibers per cell for 20 cells. Fluorescence intensity for nuclear BrdU signal (arbitrary units, A.U. in %) using ImageJ, based on Cb, determined on 50 cells. Representative results as s.e.m. from at least two independent experiments.

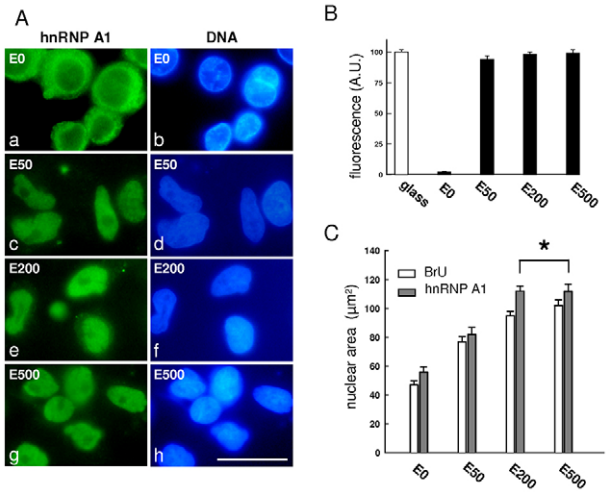

Fig. 6. hnRNP A1 nuclear concentration with respect to substrate elasticity. (**A**) Cells after 4 hours of culture on E0, E50, E200 and E500 cells with anti-hnRNP A1 (a,c,e,g) and counterstained with Hoechst 33258 (b,d,f,h). Scale bar: 20 µm. (**B**) Fluorescence intensity for nuclear hnRNP A1 signal (arbitrary units, A.U. in %) using ImageJ, based on Aa,c,e,g; 300 cells were analyzed per condition. Results are presented as s.e.m. for three independent experiments. (**C**) Quantitative data of nuclear area (in μm^2) determined using ImageJ, based on images given in Fig. 5Ab,d,f,h and here in Ab,d,f,h. 400 cells were measured in each condition. Results are presented as s.e.m. for three independent experiments; *statistically no significant difference ($P<0.05$, ANOVA).

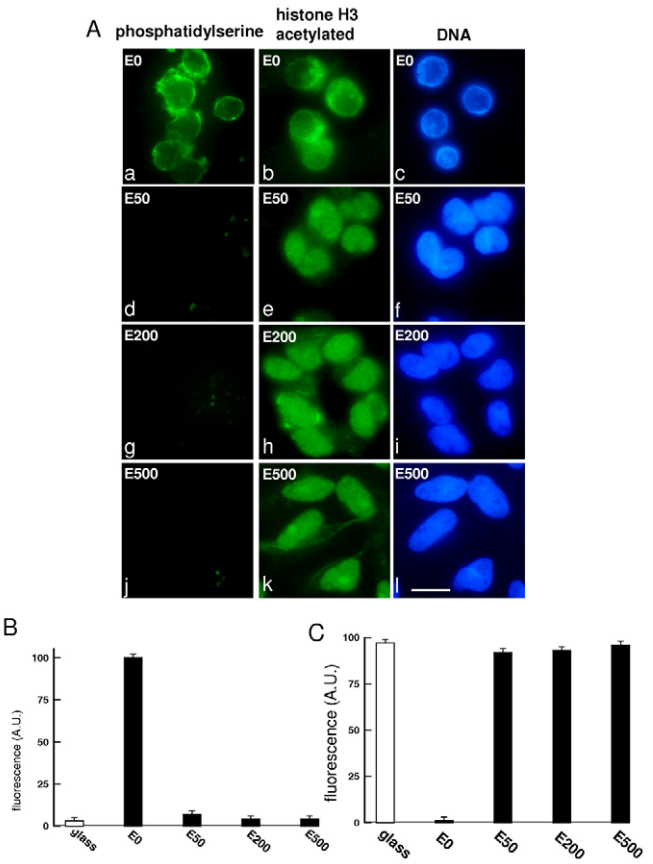

Fig. 7. Histone H3-K14 acetylation versus substrate elasticity. (**A**) After 4 hours of culture on E0, E50, E200 and E500 films, cells were tested with the apoptosis kit (a,d,g,j) and immunolabeled with anti-histone H3-K14 (b,e,h,k) and counterstained with Hoechst 33258 (c,f,i,l). Scale bar: 20 µm. (**B**) Fluorescence intensity for phosphatidyserine signal (arbitrary units, A.U. in %) using ImageJ, based on Aa,d,g,j. (**C**) Fluorescence intensity for nuclear histone H3-K14 signal (arbitrary units, A.U. in %) using ImageJ, based on Ab,e,h,k; 300 cells were analyzed in B and C. Results are presented as s.e.m. for two independent experiments.

of cells, yet it was not detected in the nucleus of interphase cells (Fig. 6Aa,B). By contrast, for cells cultured on E50, E200 and E500 films, the hnRNP A1 protein was concentrated within the nuclei (Fig. 6Ac,e,g and Fig. 6B). Similarly, cells cultured on 0/2, 0/5 and 0/12 films and on a glass surface showed that the hnRNP A1 protein was concentrated in the nucleus (data not shown). Because hnRNP A1 concentration in the nucleus is correlated with the observed transcription activation, the presence of hnRNP A1 in the nucleus might be substrate-stiffness-dependent. Transcription activation on the E50 films corresponded to that observed for replication inhibition, suggesting an uncoupled contribution from substrate elasticity to the regulation of replication and transcription activities.

Histone H3-K14 acetylation correlates with nuclei decondensation and transcription

It is also important to emphasize that the nucleus of cells adhering to E0 film remains very small (Fig. 6Ab,C, Fig. 7Ac) with highly condensed chromatin. In addition, fluorescent phosphatidylserine assays to directly count apoptotic cells showed a high intensity of phosphatidylserine and caspase-3 signal on the soft substrate E0 (Fig. 7Aa,B, supplementary material Fig. S5Ba, supplementary material Fig. S5C). These types of cell characteristics are prone to apoptosis. By contrast, increasing substrate stiffness (E50, E200 and E500 film substrates) leads to an increase in nuclear area (Fig. 6Ad,f,h, Fig. 7Af,i,l, Fig. 6C) with absence of phosphatidylserine (Fig. 7Ad,g,j and Fig. 7B) and caspase-3 signal (supplementary material Fig. S5Bc,e,g, supplementary material Fig. S5C) and correlates with the acquisition of transcriptional competence (Fig. 5Ac,e,g,B for BrU; Fig. 6Ac,e,g,B for hnRNP A1).

One question that arises from these observations is how an increase in the substrate stiffness renders the nuclei competent for transcriptional activity. Histone H3 hyperacetylation in its promoter region and other regulatory *cis*-elements are well known to be transcription-permissive (Kurdistani et al., 2004). Thus, we checked whether substrate elasticity affected histone H3 hyperacetylation activity in relationship to nuclei transcriptional competence. Immunofluorescence analyses of cells cultured for 4 hours on the soft substrate E0 showed absence of nuclear acetylated histone H3 (Fig. 7Ab,C). By contrast, on E50, E200 and E500 substrates, acetylated forms of histones H3 were detected (Fig. 7Ae,h,k, and Fig. 7C) within less dense nuclei (Fig. 7Af,i,l). These data suggest that substrates of increased stiffness (above 50 kPa) induced histone H3 acetylation and are closely correlated both with nuclei decondensation and cell transcriptional competence.

Discussion

All the results reported above are summarized schematically in Fig. 8. Cell internal architecture, via its highly dynamic interaction with the ECM, is able to sense mechanical environmental cues and to induce specific biochemical signals. Recently, 2D and 3D culture matrices, with elastic moduli comparable to those of in vivo tissues,

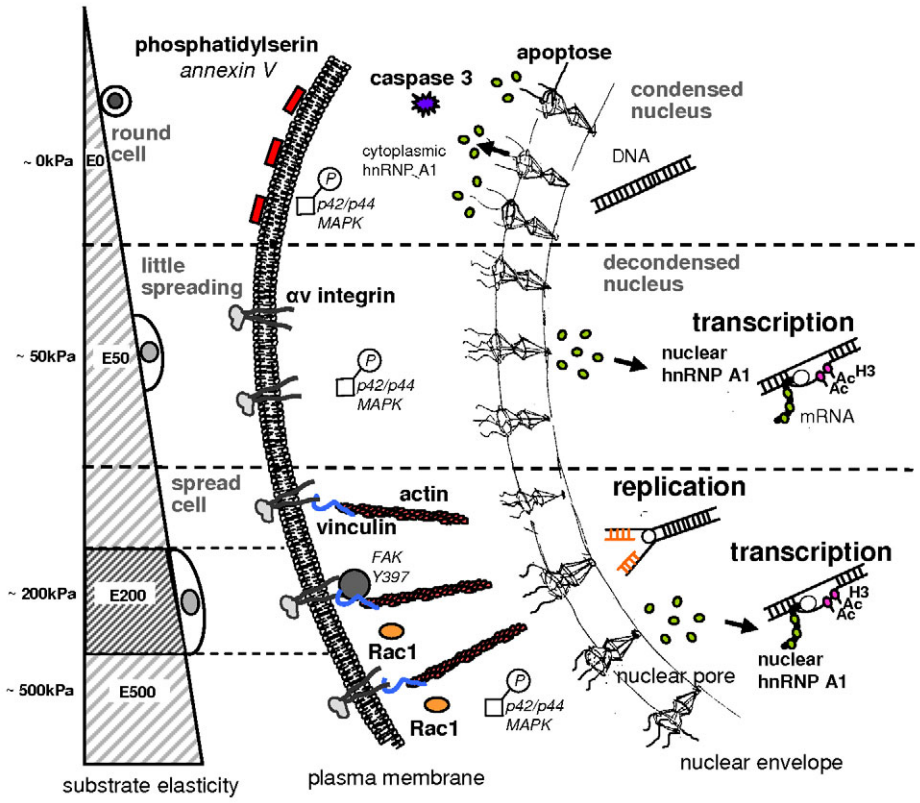

Fig. 8. Cartoon summarizing the uncoupled contribution of substrate elasticity in regulation of replication and transcription in PtK2 cells. Substrate stiffness of 500 kPa does not interfere with vinculin FA assembly or MAPK phosphorylation, but induces inhibition of FAK phosphorylation. This demonstrates that replication and transcription are dispensed from these signals (E500). In response to a substrate with a stiffness of 200 kPa: (i) FAK and MAPK are activated; (ii) transcription activity and hnRNPA1 nuclear concentration both correlate with histone H3 acetylation and DNA decondensation; and (iii) a sequential relationship between Rac1, vinculin adhesion assembly and replication becomes efficient (E200). Substrate stiffness corresponding to 50 kPa inhibits FAK phosphorylation, Rac1, vinculin assembly and stress fiber formation. The absence of actin fiber and vinculin contacts inhibits replication but does not affect transcription (E50). Soft substrate (0 kPA) is a non-permissive system for which all the nuclear functions are inhibited and cells are apoptotic (E0).

were proposed (Levental et al., 2007). Until now, it remains unclear whether substrate stiffness affects major nuclear functions such as replication and transcription through mechano-transduction pathways. In the present study, we investigated the potential role of substrate stiffness in these fundamental nuclear functions and tried to establish a possible correlation with FA signaling. We used $(PLL/HA)_{24}$ films capped by $(PSS/PAH)_n$ layers to build synthetic matrices of defined stiffness (E_{ap} of 0-500 kPa) (Francius et al., 2007). We demonstrated that the amount of FBS deposited on the surface does not depend of the number of polyelectrolyte multilayers. Because only the rigidity changes between the different polyelectrolyte multilayers used in this study, the film stiffness is probably at the origin of the cell adhesion processes. This hypothesis agrees with a recent study, demonstrating that MDCK cells can sense the substratum rigidity to a sufficient extent to induce β1-integrin activation and clustering, allowing actin organization and downstream activation events to occur (Wei et al., 2008). In our present study, low rigidity above 50 kPa is sufficient for αv-integrin engagement, allowing little cell spreading.

Vinculin assembly and formation of actin stress fibers were inhibited when cells were cultured on E0 and E50 films. This is consistent with the general changes in cell FA assembly observed as matrix stiffness increases (Ren al., 2008). However, to illustrate this cellular effect, E_{ap} values measured for our substrate model are tenfold higher than values found for polyacrylamide gels. For example, FAs and organization of the cytoskeleton were induced for mesenchymal stem cells at stiffness values of 34 kPa (Engler et al., 2006). These differences could be due to the stratified geometry of our substrate not being as isotropic as polyacrylamide gels. In addition, we could not exclude flow and creep phenomena of the film, and also a lateral cell pulling over several microns. It was previously reported that tyrosine phosphorylation increased at the adhesion sites of cells on stiff surfaces (Pelham and Wang, 1997; Giannone and Sheetz, 2006) and that the level of FAK-Y397 phosphorylation was progressively dependent on substratum rigidity (particularly at 390 Pa) on polyacrylamide gel for MDCK (Wei et al., 2008). In the present system, FAK-Y397 was only phosphorylated at around 200 kPa (E200) and again activated on the hard substratum (0/2, 0/5 and 0/12 and glass surfaces). These rigid materials (like culture plastic) are well known to favor the activation of many cell functions. Non-linear cell responses have already been described, whereby small changes in the matrix stiffness led to dramatic changes in the cell phenotype. For instance, mesenchymal stem cells expressed MyoD and CBFα-1 for rigidities of 11 kPa and 34 kPa, respectively (Engler et al., 2006). For the particular cell type and substrate model used here, FAK-Y397 was sensitive to small changes in the substrate stiffness, at least in the low-elasticity domain (0-500 kPa). This observation suggests that PtK2 epithelial cells possess an optimal window of elasticity for FAK-Y397 activation.

Using synchronized mitotic cells, we found that for the E50 substrate the inhibition of vinculin assembly is accompanied by inhibition of replication. To gain mechanistic insight into these two activities, the effect of an inhibitor (NSC23766) of the Rac1 candidate signaling pathway was investigated in cells synchronized by mitotic shake-off. Inhibition of Rac1 by this drug concomitantly obstructed vinculin assembly, actin stress and initiation of replication. Interestingly, like NSC23766, E50 substrate also inhibits Rac1 activity. Thus, we propose a sequential relationship between Rac1, vinculin assembly and replication becoming efficient at a critical elasticity (above 200 kPa). Our results differed from other investigations that used cytochalasin D to

disrupt post-mitotic actin fibers. Those authors found that actin disruption leads to inhibition of FA assembly and FAK-Y397 autophosphorylation without inhibiting entry into S phase. This could be attributable to the pre-existing cyclin D that was sufficient to drive cell-cycle progression past the M-G1 border (Margadant et al., 2007; Assoian, 1997).

During the cell cycle, natural regulation of replication and transcription occurs. In S phase both replication and transcription are active (low transcriptional activity). During gene expression, transcription sites play a role in chromatin opening, allowing the transcriptional machinery access to specific DNA sequences to initiate replication (Hassan et al., 1994; Kohzaki et al., 2005). It is important to emphasize that soft substrates induce, throughout the time period normally required to S-phase onset, an uncoupled replication-transcription response: transcription sites are visualized whereas replication is inhibited. In this range of elasticity, it is possible that the transcriptional machinery alone is not sufficient to initiate replication but requires at least the contribution of actin fiber and vinculin structures. Transcription was inhibited on the very soft substrates (E0) whereas it was active on stiffer substrates (E50). We demonstrated that above about 50 kPa, transcription was correlated with αv-integrin engagement, together with low cell spreading and with increases in nuclear area and histone H3 hyperacetylation (Rose et al., 2005). Our data are in accordance with a recent study demonstrating that three-dimensional ECM-induced cell rounding directly controls histone deacetylation and chromatin condensation in mammary epithelial cells (Le Beyec et al., 2007). In that work, disruption of the actin cytoskeleton with cytochalasin D induced cell rounding and histone deacetylation. This result strengthens the concept that actin forms a physical connection between sites of cell adhesion and the ECM, transducing mechanical signals to the interior of the nucleus (Le Beyec et al., 2007). In our present work, it is clear that substrate elasticity plays a role in the transcription competence, suggesting a connection between substrate and nucleus. However, in our system, this connection dispenses with the need for actin fibers and vinculin structures. Other physical pathways could be involved in coordinating this activity. In addition, below 50 kPa, the nucleus is strongly condensed and cells are apoptotic. Kim and co-workers demonstrate that apoptosis acts as a transcriptional repressor (Kim et al., 2004). Thus, relationship between substrate elasticity, apoptotic cellular processes and transcription can be suggested.

Conclusion

In this work, relationships between substrate elasticity with replication and transcription were investigated. Soft substrate (E0) is a non-permissive system because all the nuclear functions are inhibited and cells are apoptotic. Cell adhesion, in response to a substrate with a stiffness of 200 kPa, enables integrin activation. Sequential relationship between Rac1, vinculin adhesion assembly and replication becomes efficient and accompanied by activation of FAK and MAPK, activation of transcription, hnRNP A1 nuclear accumulation and histone H3 acetylation correlated with chromatin decondensation. Substrate stiffness corresponding to 500 kPa does not interfere with vinculin assembly or MAPK phosphorylation, but does inhibit FAK phosphorylation, suggesting that this signal is not necessary for replication and transcription. Substrate stiffness corresponding to 50 kPa inhibits FAK, Rac1 activity, vinculin assembly and actin fiber formation, leading to the inhibition of replication, but it does not affect transcription, hnRNPA1 nuclear concentration and histone H3 acetylation correlated with chromatin decondensation and integrin activation. On the basis of our data, we propose an uncoupled contribution of substrate elasticity to the regulation of replication and transcription. However, the selective properties for particular substrate elasticity are probably cell-type-dependent. For example, neuronal cells express a specific phenotype marker at an elasticity value of several hundred pascals, whereas tendon and cartilage do so at a megapascal value (Levental et al., 2007). It is highly probable that substrate elasticity plays a selective role in these nuclear activities so important in tissue homeostasis. The physiological significance of these nuclear activities in the regulation of apoptosis, differentiation and the propensity for tumorigenesis still needs further investigations.

Materials and Methods

Polyelectrolytes

PLL (MW=5.7×10^4 Da, Sigma, St Quentin Fallavier, France), fluorescein isothiocyanate labeled poly(L-lysine) (PLL^{FITC}, MW=5.0×10^4 Da, Sigma) and HA (MW=4.0×10^5 Da, BioIberica, Barcelona) were used for buildup of $(PLL/HA)_{24}$ films. PSS (MW=7.0×10^4 Da, Sigma), rhodamine-labeled PSS (PSS^{rho}, MW=5.0×10^4 Da, Sigma) and PAH (MW=7.0×10^4 Da, Sigma) were used for buildup of $(PSS/PAH)_n$ top films (where n corresponds to the number of layer pairs), which were deposited on $(PLL/HA)_{24}$ stratum. PLL, PLL^{FITC}, HA, PSS, PSS^{rho}, and PAH were dissolved at 1 mg/ml in buffer solution containing 150 mM NaCl and 20 mM of tris(hydroxymethyl)-aminomethane (TRIS, Merck) at pH 7.4. During film construction, all rinsing steps were performed with 150 mM NaCl and 20 mM TRIS aqueous solution at pH 7.4. $(PLL/HA)_{24}$ strata were prepared using dipping machine (Dipping Robot DR3, Riegler & Kirstein, Berlin, Germany), on glass slides (VWR Scientific, Fonteney sous Bois, France). $(PSS/PAH)_n$ top films were prepared manually.

Film characterization

CLSM observations were performed with Zeiss LSM 510 microscope using 40× 1.4 oil immersion lens. FITC-fluorescence was detected after excitation at 488 nm with cut-off dichroic mirror 488 nm and emission band-pass filter 505-530 nm. Rho-fluorescence was detected after excitation at 543 nm, dichroic mirror 543 nm, and emission long pass filter 585 nm.

Quartz crystal microbalance

QCM consists in measuring resonance frequency (f) of quartz crystal after polyelectrolyte adsorption, in comparison with resonance frequency of crystal. Crystal used here is coated with 50-nm thick SiO_2. Crystal is excited at its frequency and measurements at frequency of 15 MHz (third overtone, ν=3). Changes in resonance frequency, Δf, during each adsorption step are measured. A shift in Δf can be associated with variation of mass adsorbed on crystal. This mass m was calculated by the Sauerbrey relation $m=-C(\Delta f/\nu)$, where C is a constant characteristic of crystal (C=17.7 ng cm^{-2} Hz^{-1}) (Sauerbrey, 1959). We monitored deposition of 10% FBS on bare crystal and on polyelectrolyte multilayer.

Cell and synchronization

PtK2 cells (CCL-56, LGC Standards, UK) were grown in RPMI-1640 medium (Invitrogen) supplemented with 100 μg/ml penicillin, 100 μg/ml streptomycin (Invitrogen,) and 10% FBS (Invitrogen), and maintained at 37°C with 5% CO_2. Cells were synchronized by mechanical shake-off. Three days prior to synchronization, cells were replated at 1.2×10^4 per cm^2. Mitotic cells were centrifuged (700 ***g***, 5 minutes), resuspended in culture medium, and replated at 1.2×10^4 per cm^2 from surfaces. For Rac1 inhibitor treatment, cells were cultured with 100 μM NSC 23766 for 0-7 hours after synchronization.

Cell adhesion

MTT test

Cells were plated on multilayered or bare glass samples placed in 24-well plates (Nunc) at 1×10^5 per cm^2. After 4 hours of culture, non-attached cells were removed by two washes with 37°C phosphate-buffered saline (PBS). Plates were incubated with 500 μl per well of MTT solution (0.1% w/v 3-(4,5-dimethylthiozol-2-yl)-2,5-diphenyltetrazolium bromide in PBS) and incubated for 180 minutes at 37°C. Medium was displaced by 500 μl DMSO. OD was measured at 570 nm.

Acid phosphatase assay

Cells were seeded on multilayered or bare glass samples placed in 24-well plates (Nunc) at 1×10^5 per cm^2. After 4 hours of culture, unattached cells were removed after two washes with PBS at 37°C and incubated with *p*-nitrophenyl phosphate (Sigma, Steinheim) at 1 mg ml^{-1} in 0.1 M sodium acetate (pH 5.5) and 0.1% Triton X-100 for 3 hours at 37°C in 5% CO_2. Reaction was stopped by 1 N sodium hydroxide. Absorbance was measured at 405 nm. A value of 100% was ascribed to the acid phosphatase activity of cells on glass.

Immunolabeling

Cells were seeded on surfaces (multilayered films or bare glass samples placed in 24-well plates (Nunc) at 1×10^5 (asynchronized) or 1.2×10^4 per cm^2 (synchronized). Cells were fixed in 3.7% (w/v) paraformaldehyde (PFA) in PBS for 15 minutes, and fixed/permeabilized in 3.7% (w/v) PFA in PBS plus 0.1% Triton X-100 for 10 minutes. Cells were blocked with 10% decomplemented FBS (Invitrogen). For measurement of αv-integrin, vinculin and hnRNP A1, cells were incubated with αv-integrin (1:100; Santa Cruz Biotechnology), anti-vinculin (1:100; clone hVin-1, Sigma) and anti-hnRNP A1 (1:100; clone 9H10, Abcam). After washings with PBS, cells were incubated with FITC-conjugated secondary antibody (1:500; AnaSpec, Fremont, CA). For acetyl-histone H3, cells were incubated with anti-acetyl-histone-H3-Lys14 (1:100; Millipore) and then incubated with FITC- or TRITC-conjugated secondary antibody (1:500; AnaSpec). For Rac1, cells were incubated with anti-Rac1 (1:100, Millipore), for caspase-3, with anti-caspase-3 (1:50, Cell Signaling), for actin staining with TRITC-phalloidin (1 μg ml^{-1}; Sigma), and for DNA with Hoechst 33258 (20 μg ml^{-1}, Sigma).

Replication

Cells were seeded on surfaces at 1×10^5 (asynchronized) or 1.2×10^4 per cm^2 (synchronized). Cells were incubated with BrdU for 15 minutes (37°C) (1:500; RPN 201, GE Healthcare Europe). Cells were fixed/permeabilized in 3.7% PFA in PBS plus 0.5% Triton X-100 for 15 minutes. After washing with PBS, cells were incubated with anti-BrdU and DNase for 1 hour at 37°C (1:100; RNP 202, GE Healthcare Europe). After washings with PBS, cells were incubated with FITC-conjugated secondary antibody (1:500; AnaSpec).

Transcription

Cells were seeded on surfaces: 1×10^5 (asynchronized) or 1.2×10^4 per cm^2 (synchronized). and washed in PB buffer (100 mM CH_3-COOK, 30 mM KCl, 10 mM Na_2HPO_4, 1 mM $MgCl_2$, 1 mM DTT, 1 mM ATP, pH 7.4) on ice and incubated with 0.05% Triton X-100 in phosphate buffer (PB) for 2 minutes on ice. Cells were washed with PB, then cells were incubated with transcription mix (0.1 mM CTP, 0.1 mM UTP and 0.1 mM GTP in PB) containing 0.1 mM BrU (Sigma) for 20 minutes at 33°C. Then, cells were washed with PB and permeabilized with 0.2% Triton X-100 in PB for 3 minutes. Cells were fixed with 3.7% PFA in PB for 15 minutes followed by washing in PB. Cells were washed in PBS and the incorporated Br-UTP was detected using anti-BrdU (1:100; monoclonal anti-BrdU, clone BY-33, Sigma). Cells were incubated with FITC-conjugated secondary antibody (1:500; AnaSpec).

Apoptosis

Cells were seeded at 1×10^5 or 1.2×10^4 per cm^2. Annexin V binding was carried out using the Vybrant Apoptosis Assay Kit (Molecular Probes) according to the manufacturer's instructions. Cells were analyzed by fluorescence microscopy.

Microscopy

Samples were mounted in VectaShield (Vector Laboratories, Burlingame, CA). Fluorescence was visualized with Nikon Elipse TE200 (objective lenses 63× 1.4 NA). Images were acquired with Nikon Digital Camera (DXM 1200 or DS-Q11MC with ATC-1 or NIS-Elements softwares). Pictures were processed with ImageJ (http://rsb.info.nih.gov/ij/).

Western blot

Cells were seeded on surfaces (Nunc) at 2×10^5 per cm^2 and incubated for 4 hours in culture medium at 37°C and at end of incubation treated with 1% of 0.2 M sodium orthovanadate (Sigma). Cells were lysed in 20 mM Tris-base, pH 8, 0.15 M NaCl, 2 mM EDTA, 1% NP-40, 10% glycerol, 1 mM sodium orthovanadate containing 1% of protease inhibitor cocktail; Sigma). Extraction mixtures were rocked at 4°C for 1 hour and centrifuged (5 minutes, 7000 ***g*** at 4°C). Protein concentration was determined using DC protein assay (BioRad). Equal amounts of total protein extracts were subjected to SDS PAGE (NuPAGE, Invitrogen, Cergy Pontoise, France) and transferred onto nitrocellulose membranes (Iblot Transfer Stack, Invitrogen) blocked in T-TBS (0.1% Tween 20, 50 mM Tris-base, pH 7.6, 0.15 M NaCl) containing 1% BSA (Euromedex, France) and probed overnight at 4°C with primary antibody: FAK-Y397-*P* (1:1000; BD Transduction laboratories, Lexington, KY), FAK (1:1000; Santa Cruz Biotechnology), phosphorylated p44/p42 MAPK (1:2000; Cell Signaling), p44/p42 MAPK (1:1000; Cell Signaling, USA). Blots were incubated for 2 hours with HRP-conjugated anti-rabbit, anti-mouse antibodies (1:5000; GE Healthcare). Bands were detected using an enhanced chemiluminescence (ECL) kit (GE Healthcare). Autoradiographs were quantified with Kodak Digital Science 10 Software. Representative mean values were of at least three independent experiments with standard errors (four time-points per band). A value of 1 was attributed to cells on glass.

We are indebted Jean-Noël Freund (INSERM U682, Strasbourg, France) and Ludovic Richert (CNRS 7213, Faculté de Pharmacie, Strasbourg, France) for stimulating discussions, and Christian Ringwald (INSERM U977) for QCM experiments. The study was supported by Grants from Agence Nationale de la Recherche (Tecscan, 'Subvacel Project') and 'Cancéropôle du Grand Est'. P.L. is indebted to Hôpitaux Universitaires de Strasbourg for financial support. We are grateful to Jérôme Mutterer of Institut de Biologie Moléculaire des Plantes, CNRS/Université de Strasbourg, France for his contribution with CLSM. The CLSM platform used in this study was co-financed by Région Alsace, Université de Strasbourg, and Association pour la Recherche sur le Cancer. L.K. is indebted to Faculté de Chirurgie Dentaire of Strasbourg, for financial support.

Supplementary material available online at
http://jcs.biologists.org/cgi/content/full/123/1/29/DC1

References

Assoian, R. K. (1997). Anchorage-dependent cell cycle progression. *J. Cell Biol.* **136**, 1-4.

Balby, M. J., Gadegaard, N., Herzyl, P., Sutherland, D., Agheli, H., Wilkinson, C. D. and Curtis, A. S. (2007). Nanomechanotransduction and interphase nuclear organization influence on genomic control. *J. Cell Biochem.* **102**, 1234-1244.

Biggs, M. J., Richards, R. G., Gadegaard, N., Wilkinson, C. D. and Dalby, M. J. (2007). Regulation of implant surface cell adhesion: characterization and quantification of S-phase primary osteoblast adhesions on biomimetic nanoscale substrates. *J. Orthop. Res.* **25**, 273-282.

Boura, C., Muller, S., Vautier, D., Dumas, D., Schaaf, P., Voegel, J. C., Stoltz, J. F. and Menu, P. (2005). Endothelial cell-interactions with polyelectrolyte multilayer films. *Biomaterials* **22**, 4568-4575.

Burridge, A. D. and Wennerberg, K. (2004). Rho and Rac take center stage. *Cell* **116**, 167-179.

Decher, G. (1997). Fuzzy nanoassemblies: Toward layered polymeric multicomposites. *Science* **277**, 1232-1237.

Discher, D. E., Janmey, P. and Wang, Y. L. (2005). Tissue cells feel and respond to the stiffness of their substrate. *Science* **310**, 1139-1143.

Dreyfuss, G., Matunis, M. J., Piñol-Roma, S. and Burd, C. G. (1993). hnRNP proteins and the biogenesis of mRNA. *Annu. Rev. Biochem.* **62**, 289-321.

Dubreuil, F., Elsner, N. and Fery, A. (2003). Elastic properties of polyelectrolyte capsules studies by atomic-force microscopy and RICM. *Eur. Phys. J. E* **12**, 215-221.

Engler, A. J., Griffin, M. A., Sen, S., Bonnemann, C. G., Sweeney, H. L. and Discher, D. E. (2004). Myotubes differentiate optimally on substrates with tissue-like stiffness: pathological implications for soft or stiff microenvironments. *J. Cell Biol.* **166**, 877-887.

Engler, A. J., Sen, S., Sweeney, H. L. and Discher, D. E. (2006). Matrix elasticity directs stem cell lineage specification. *Cell* **126**, 677-689.

Engler, A. J., Carag-Krieger, C., Johnson, C. P., Raab, M., Tang, H. Y., Speicher, D. W., Sanger, J. W., Sanger, J. M. and Discher, D. E. (2008). Embryonic cardiomyocytes beat best on a matrix with heaet-like elasticity: scar-like rigidity inhibits beating. *J. Cell Sci.* **121**, 3794-3802.

Ferreira, J. A., Carmo-Fonseca, M. and Lamond, A. I. (1994). Differential interaction of splicing snRNPs with coiled bodies and interchromatin granules during mitosis and assembly of daughter cell nuclei. *J. Cell Biol.* **126**, 11-23.

Ferreira, J., Paolella, G., Ramos, C. and Lamond, A. I. (1997). Spatial organization of large-scale chromatin domains in the nucleus: a magnified view of single chromosome territories. *J. Cell Biol.* **139**, 1597-1610.

Francius, G., Hemmerlé, J., Ohayon, J., Schaaf, P., Voegel, J. C., Picart, C. and Senger, B. (2006). Effect of crosslinking on the elasticity of polyelectrolyte multilayer films measured by colloidal probe AFM. *Microsc. Res. Tech.* **69**, 84-92.

Francius, G., Hemmerlé, J., Ball, V., Lavalle, P., Picart, C., Voegel, J. C., Schaaf, P. and Senger, B. (2007). Stiffening of soft polyelectrolyte architectures by multilayer capping evidenced by viscoelastic analysis of AFM indentation measurements. *J. Phys. Chem. C* **111**, 8299-8306.

Garza, J. M., Schaaf, P., Muller, S., Ball, V., Stoltz, J. F., Voegel, J. C. and Lavalle, P. (2004). Multicompartment films made of alternate polyelectrolyte multilayers of exponential and linear growth. *Langmuir* **20**, 7298-7302.

Georges, P. C., Miller, W. J., Meaney, D. F., Sawyer, E. S. and Janmey, P. A. (2006). Matrices with compliance comparable to that of brain tissue select neuronal over glial growth in mixed cortical cultures. *Biophys. J.* **90**, 3012-3018.

Giannone, G. and Sheetz, M. P. (2006). Substrate rigidity and force define form through tyrosine phosphatise and kinase pathways. *Trends Cell Biol.* **16**, 213-223.

Gieni, S. and Hendzel, M. J. (2008). Mechanotransduction from the ECM to the Genome: are the pieces now in place? *J. Cell Biochem.* **104**, 1964-1987.

Gross, I., Duluc, I., Benameur, T., Calon, A., Martin, E., Brabletz, T., Kedinger, M., Domon-Dell, C. and Freund, J. N. (2008). The intestine-specific homeobox gene Cdx2 decreases mobility and antagonizes dissemination of colon cancer cells. *Oncogene* **27**, 107-115.

Hassan, A., Errington, R. J., White, N. S., Jackson, D. A. and Cook, P. R. 1994. Replication and transcription sites are colocalized in human cells. *J. Cell Sci.* **107**, 425-434.

Huang, C., Jacobson, K. and Schaller, M. D. (2004). MAP kinases and cell migration. *J. Cell Sci.* **117**, 4619-4628.

Kim, W., Kook, S., Kim, D. J., Teodorof, C. and Song, W. K. (2004). The 31-kDa caspase-generated cleavage product of p130cas functions as a transcriptional repressor of E2A in apoptotic cells. *J. Biol. Chem.* **279**, 8333-8342.

Kohzaki, H. and Murakami, Y. (2005). Transcription factors and DNA replication origin selection. *BioEssays* **27**, 1107-1116.

Kornberg, L. J., Earp, H. S., Turner, C. E., Prockop, C. and Juliano, R. L. (1991). Signal transduction by integrins: increased protein tyrosine phosphorylation caused by clustering of beta 1 integrins. *Proc. Natl. Acad. Sci. USA* **88**, 8392-8396.

Kurdistani, S. K., Tavazoie, S. and Grunstein, M. (2004). Mapping global histone acetylation patterns to gene expression. *Cell* **117**, 721-733.

Le Beyec, J., Wu, R., Lee, S. Y., Nelson, C. M., Rizki, A., Alcaraz, J. and Bissell, M. J. (2007). Cell shape regulates global histone acetylation in human mammary epithelial cells. *Exp. Cell Res.* **313**, 3066-3075.

Levental, I., Georges, P. C. and Janmey, P. A. (2007). Soft biological materials and their impact on cell function. *Soft Matter* **3**, 299-306.

Lo, C. M., Wang, H. B., Dembo, M. and Wang, Y. L. (2000). Cell movement is guided by the rigidity of the substrate. *Biophys. J.* **79**, 144-152.

Margadant, C., van Opstal, A. and Boonstra, J. (2007). Focal adhesion signalling and actin stress fibers are dispensable for progression through the ongoing cell cycle. *J. Cell Sci.* **120**, 66-76.

Maxwell, C. A. and Hendzel, M. J. (2001). The integration of tissue structure and nuclear function. *Biochem. Cell Biol.* **79**, 267-274.

Mendelsohn, J. D., Yang, S. Y., Hiller, Y., Hochbaum, A. I. and Rubner, M. F. (2003). Rational design of cytophilic and cytophobic polyelectrolyte multilayer thin films. *Biomacromolecules* **4**, 96-106.

Meredith, D. O., Owen, G. R., ap Gwynn, I. and Richards, R. G. (2004). Variation in cell-substratum adhesion in relation to cell cycle phases. *Exp. Cell Res.* **293**, 58-67.

Mitchison, J. M. (1971). The biology of the cell cycle. Cambridge University Press: Cambridge.

Nobes, C. D. and Hall, A. (1995). Rho, Rac and cdc42 GTPases regulate the assembly of multimolecular focal complexes associated with actin stress fibers, Lamelliopodia, and filopodia. *Cell* **81**, 53-62.

Pardee, A. B. (1989). G1 events and regulation of cell proliferation. *Science* **246**, 603-608.

Paszek, M. J., Zahir, N., Johnson, K. R., Lakins, J. N., Rozenberg, G. I., Gefen, A., Reinhart-King, C. A., Margulies, S. S., Dembo, M., Boettiger, D. et al. (2005). Tensional homeostasis and the malignant phenotype. *Cancer Cell*. **8**, 241-254.

Pelham, R. J., Jr and Wang, Y. L. (1997). Cell locomotion and focal adhesions are regulated by substrate flexibility. *Proc. Natl. Acad. Sci. USA* **94**, 13661-13665.

Picart, C., Senger, B., Sengupa, K., Dubreuil, F. and Fery, A. (2007). Measuring mechanical properties of polyelectrolyte multilayer thin films: novel methods based on AFM and optical techniques. *Colloids and Surfaces A* **303**, 30-36.

Piñol-Roma, S. and Dreyfuss, G. (1991). Transcription-dependent and transcription-independent nuclear transport of hnRNP proteins. *Science* **253**, 312-314.

Ren, K. F., Crouzier, T., Roy, C. and Picart, C. (2008). Polyelectrolyte multilayer films of controlled stiffness modulate myoblast cell differentiation. *Adv. Funct. Mater.* **18**, 1378-1389.

Richert, L., Engler, A. J., Discher, D. E. and Picart, C. (2004). Elasticity of native and cross-linked polyelectrolyte multilayer films. *Biomacromolecules* **5**, 1908-1916.

Rizzi, S. C., Ehrbar, M., Halstenberg, S., Raeber, G. P., Schmoekel, H. G., Hagenmuller, H., Muller, R., Weber, F. E. and Hubbell, J. A. (2006). Recombinant protein-co-PEG networks as cell-adhesive proteolytically degradable hydrogel matrixes. Part II: Biofunctional characteristics. *Biomacromolecules* **7**, 3019-3029.

Roovers, K. and Assoian, R. K. (2003). Effects of rho kinase and actin stress fibers on sustained extracellular signal-regulated kinase activity and activation of G(1) phase cyclin-dependent kinases. *Mol. Cell. Biol.* **23**, 4283-4294.

Rose, J. L., Huang, H., Wray, S. F. and Hoyt, D. G. (2005). Integrin engagement increases histone H3 acetylation and reduces histone H1 association with DNA in murine Lung endothelial cells. *Mol. Pharmacol*. **68**, 439-446.

Sauerbrey, G. Z. (1959). Verwendung von Schwingquartzen zur Wägung dünner Schichten und zur Mikrowägung. *Phys*. **155**, 206-222.

Schaller, M. D., Hildebrand, J. D. and Parsons, J. T. (1999). Complex formation with focal adhesion kinase: a mechanism to regulate activity and subcellular localization of Src kinases. *Mol. Biol. Cell* **10**, 3489-3505.

Snedeker, J. G., Barbezat, M., Niederer, P., Schmidlin, F. R. and Farshad, M. (2005). Strain energy density as a rupture criterion for the kidney: impact tests on porcine organs, finite element simulation, and a baseline comparison between human and porcine tissues. *J. Biomech.* **38**, 993-1001.

Shimi, T., Pfleghaar, K., Kojima, S., Pack, C. G., Solovei, I., Goldman, A. E., Adam, S. A., Shumaker, D. K., Kinjo, M., Cremer, T. et al. (2008). The A- and B-type nuclear lamin networks: microdomains involved in chromatin organization and transcription. *Genes Dev*. **22**, 3409-3421.

Vautier, D., Chesné, P., Cunha, C., Calado, A., Renard, J. P. and Carmo-Fonseca, M. (2001). Transcription-dependent nucleocytoplasmic distribution of hnRNP A1 protein in early mouse embryos. *J. Cell Sci.* **114**, 1521-1531.

Wang, F., Weaver, V. M., Petersen, O. W., Larabell, C. A., Dedhar, S., Briand, P., Lupu, R. and Bissell, M. J. (1998). Reciprocal interaction between □1-integrin and epidermal growth factor receptor in three-dimensional basement membrane breast cultures: a different perspective in epithelial biology. *Proc. Natl. Acad. Sci. USA* **95**, 14821-14826.

Wang, N., Tytell, J. D. and Ingber, D. E. (2009). Mechanotransduction at a distance: mechanically coupling the extracellular matrix with the nucleus. *Nat. Rev. Mol. Cell. Biol.* **10**, 75-82.

Wei, W. C., Lin, H. H., Shen, M. R. and Tang, M. J. (2008). Mechanosensing machinery for cells under low substratum rigidity. *Am. J. Physiol. Cell Pysiol.* **295**, 1579-1589.

Wong, J. Y., Velasco, A., Rajagopalan, P. and Pham, Q. (2003). Directed movement of vascular smooth muscle cells on gradient-compliant hydrogels. *Langmuir* **19**, 1908-1913.

Wozniak, M. A., Desai, R., Solski, P. A., Der, C. J. and Keely, P. J. (2003). ROCK-generated contractility regulates breast epithelial cell differentiation in response to the physical properties of a three-dimensional collagen matrix. *J. Cell Biol*. **163**, 583-595.

Yeung, T., Georges, P. C., Flanagan, L. A., Marg, B., Ortiz, M., Funaki, M., Zahir, N., Ming, W., Weaver, V. and Janmey, P. A. (2005). Effects of substrate stiffness on cell morphology, cytoskeletal, and adhesion. *Cell Motil. Cytoskeleton* **60**, 24-34.

Journal of Cell Science